Optics & Laser Technology 41 (2009) 384–391

Contents lists available at ScienceDirect

Optics & Laser Technology

journal homepage: www.elsevier.com/locate/optlastec

Large amplitude noise reduction in ultrashort pulse trains using a power-symmetric nonlinear optical loop mirror

O. Pottiez [a,*], B. Ibarra-Escamilla [b], E.A. Kuzin [b]

[a] Centro de Investigaciones en Óptica, Fibras, Loma del Bosque 115, Col. Lomas del Campestre, 37150 León, Guanajuato, Gto, Mexico
[b] Instituto Nacional de Astrofísica, Óptica y Electrónica (INAOE), L. E. Erro 1, Tonantzintla, 72000 Puebla, Pue., Mexico

ARTICLE INFO

Article history:
Received 20 May 2008
Received in revised form
27 August 2008
Accepted 3 September 2008
Available online 23 October 2008

Keywords:
Sagnac interferometer
Fibre-optic devices
Optical signal processing

ABSTRACT

We analyse numerically the capabilities of a power-symmetric nonlinear optical loop mirror (NOLM) in the ultrashort pulse regime for high-quality amplitude regeneration of an optical signal. The device, which operates through nonlinear polarisation rotation, includes twisted, anomalous-dispersion fibre and a quarter-wave retarder. For particular adjustments of the retarder orientation, and a circularly polarised input beam, the output energy characteristic flattens near the switching energy, a property that can be used to eliminate large amplitude fluctuations in an optical signal. The group velocity mismatch between polarisation components introduced by twist is mitigated by the interplay between anomalous dispersion and the nonlinear Kerr effect, although strong twist should be avoided as it still introduces substantial pulse distortion. Contrary to other designs, where a plateau characteristic requires a large power imbalance between the counter-propagating beams, both pulses in the present scheme can be simultaneously close to fundamental solitons, which allows a substantial widening of the plateau for particular pulse parameters. Good quality, nearly transform-limited pulses are obtained in this case at the NOLM output. The device is applicable for the regeneration of ultrafast data streams in which the signal-to-noise ratio is severely deteriorated.

1. Introduction

As optical transmission systems operating at 40 Gbits/s or beyond are being developed, devices capable of handling ultrashort-pulsed signals as such high rates are needed. The nonlinear optical loop mirror (NOLM) [1], which exploits the ultrafast optical Kerr effect in fibre, is a good candidate for these tasks. Its use was proposed for applications like ultrafast switching and demultiplexing [2,3], wavelength conversion [4], pedestal suppression [5], amplitude equalisation and regeneration of optical signals [6–9], or other operations in the frame of optical signal processing [10,11] or monitoring [12]. NOLM switching can be provided either by a control beam, or by the signal itself. The latter case is considered here. In this case, and in spite of the diversity of the existing schemes, they have generally in common the use of a power imbalance between the counter-propagating beams to enable self-switching. For this purpose, some schemes rely on an asymmetric coupler in the NOLM design [1,13,14], while in others some loss (or gain) is inserted asymmetrically in the loop [6–10,12]. In other schemes, an asymmetry in the loop dispersion [15,16] or birefringence [17] is used. In these cases, the power imbalance is obtained by splitting or stretching the pulses in the loop, in such a way that their peak power undergoes different evolutions in clockwise (CW) and counter-clockwise (CCW) directions.

The transmission characteristic of a NOLM is usually a sinusoidal function of input power, whose bias is adjustable in practice through a lumped birefringent element (usually a polarisation controller, PC). A theory of the NOLM operation in the continuous-wave case was soon developed [1], and numerous numerical studies were carried out to analyse the device operation in the ultrashort pulse regime. These studies showed the outstanding properties of solitons, which can be switched entirely with minimal pulse shape distortion [1,13], cleaned and reshaped [5–9,14–17], or stabilised over long transmission links [18]. However, although the residual birefringence of the standard fibre used in the NOLM affects the bias and is responsible for a complex polarisation evolution of the beams circulating in the loop, it was not taken into account in these early studies. This simplification can be valid considering that, for long fibre loops with random birefringence, the nonlinear polarisation evolution statistically averages out for each beam, whereas the linear bias induced by residual birefringence can be compensated in practice by the empiric adjustment of a PC inserted in the loop. Still, fibre birefringence and polarisation evolution modify the NOLM operation, and a few groups tried to figure out how it happens.

* Corresponding author. Tel.: +52 4774414200; fax: +52 4774414209.
E-mail address: pottiez@cio.mx (O. Pottiez).

0030-3992/$ - see front matter © 2008 Elsevier Ltd. All rights reserved.
doi:10.1016/j.optlastec.2008.09.001

Some of the first studies of polarisation effects in NOLMs can be found in [19,20], but a comprehensive study of polarisation effects in NOLMs [21] would follow by more than a decade the funding paper by Doran et al. [1]. In [22], the first thorough study of the impairments imposed by residual birefringence on the NOLM operation was presented.

An interesting approach consists in taking advantage of polarisation effects to improve the NOLM operation. In [23], for example, control of light polarisation in the loop allows compensating for the impairments related to counter-propagating interactions. In [21], a novel NOLM design is proposed, in which a polarisation asymmetry is used instead of a power asymmetry between the counter-propagating beams. In this scheme, switching is due to nonlinear polarisation rotation instead of self-phase modulation. The polarisation states of counter-propagating beams are made different through the use of a quarter-wave retarder (QWR) inserted in the loop after one of the coupler output ports. To prevent the nonlinear polarisation evolution from averaging out for each beam, twist is applied to the fibre, which then becomes optically active and behaves like an ideal isotropic fibre [24]. Starting from the coupled nonlinear differential equations for polarisation evolution in the continuous-wave case [25], a model was proposed in [21], which enabled a thorough study of this promising device (see for example [26–28]). In comparison with conventional schemes, the proposed architecture showed up improved robustness to external perturbations, and enhanced flexibility of the transmission characteristic (which can be adjusted through controlling polarisation and birefringence). We demonstrated in particular that, when input polarisation is circular, the dynamic range can be controlled through the QWR angle. For particular values of this angle, a wide plateau appears in the output power characteristic, which enables high-quality amplitude regularisation of an optical signal. In [29], using this scheme, we were able to eliminate large amplitude fluctuations affecting a train of sub-ns optical pulses, as predicted by the model. This model, however, is valid only in the continuous-wave case, and is thus not transposable to the case of ultrashort (picosecond) pulses. In particular, it does not take into account chromatic dispersion and the group velocity mismatch between polarisation components. These effects cause changes in the pulse profile and peak power during propagation, resulting in accumulated nonlinear phase shift and polarisation rotation that are modified with respect to the continuous-wave case. Consequently, the NOLM operation in the ultrashort pulse regime will be quantitatively different from the continuous-wave regime. The performances are also expected to depend strongly on whether the soliton effect is at play in the loop or not. As a consequence, for a precise quantitative assessment of the device performances in the case of ultrashort pulses, the NOLM operation must be re-examined in this regime.

In this paper we undertake a numerical study of the NPR-based NOLM operation in the picosecond pulse regime. Anomalous dispersion is considered. We analyse in detail the device capabilities in the frame of the reduction of amplitude fluctuations, and compare its performances with those of another reported scheme, in which a large power imbalance is used to form a plateau.

2. Numerical analysis

For the continuous-wave analysis of the device operation, time-dependent effects were neglected, so that the fields were functions of one variable only, the propagation distance, z. In this case, a set of two coupled ordinary differential equations is sufficient to describe the propagation of the two polarisation components of each beam along the loop [25]. In practice, this model is valid if the fibre length is short and the pulses are long, and in this case their profile is not modified during propagation. To study the NOLM behaviour for ultrashort input pulses, however, the dependence of the fields on time t must be taken into account as well, so that each polarisation component of the counter-propagating fields is a function of the two variables z and t. The description of light propagation then requires a set of two partial differential equations, the coupled nonlinear Schrödinger equations [30]. With these equations, effects like chromatic dispersion and group velocity mismatch, which tend to modify the pulse temporal profile as it propagates, can be taken into account. In the basis of circular polarisation [C^+, C^-], these equations write as

$$\frac{\partial C^+}{\partial z} = -\frac{\Delta\beta_1}{2}\frac{\partial C^+}{\partial t} - \mathrm{j}\frac{\beta_2}{2}\frac{\partial^2 C^+}{\partial t^2} + \frac{2\mathrm{j}\gamma}{3}(|C^+|^2 + 2|C^-|^2)C^+,$$
$$\frac{\partial C^-}{\partial z} = +\frac{\Delta\beta_1}{2}\frac{\partial C^-}{\partial t} - \mathrm{j}\frac{\beta_2}{2}\frac{\partial^2 C^-}{\partial t^2} + \frac{2\mathrm{j}\gamma}{3}(|C^-|^2 + 2|C^+|^2)C^-, \quad (1)$$

where $\Delta\beta_1 = \beta_1^+ - \beta_1^-$ is the inverse group velocity mismatch, β_2 is the second-order dispersion parameter and γ is the Kerr nonlinear coefficient. Time t is referenced in a system that travels at the average group velocity $v_g = 2/(\beta_1^+ + \beta_1^-)$. Note that, for circular polarisation, the self-phase modulation (SPM) coefficient is 2/3 times smaller than the SPM coefficient γ for linear polarisation. Fibre loss is neglected, as well as higher-order dispersion and Raman self-frequency shift, a valid approximation for the parameters of the NOLM and of the pulses considered here. The split-step Fourier technique is used to numerically integrate these equations for the two beams counter-propagating in the loop.

The NOLM loop is made of a length $L = 1$ km of fibre with anomalous dispersion $D = 19$ ps/nm/km ($\beta_2 = -24.2$ ps^2/km at 1550 nm) and $\gamma = 7.5$ rad/W/km. We assume that the fibre birefringence is circular, so that the twist-induced optical activity is supposed to overcome linear birefringence. In practice, a moderate twist easily eliminates the fibre residual birefringence (whose beat length $L_B \approx 10$–50 m [31,32]). Indeed, if the fibre is twisted at a rate of N turns/m, the birefringence axes rotate at this same rate, whereas light polarisation rotates at $\sim 0.05N$ only, as the optical activity generated by twist amounts to $\sim$5% of the twist rate in silica fibre [21,33]. Even considering a moderate twist $N = 1$ turn/m, polarisation rotates at a rate of $0.95N = 0.95$ with respect to the birefringence axes, and the product $0.95NL_B \gg 1$, so that the residual birefringence averages out. The situation is different however when the fibre is wound on a spool after twisting. Bending the fibre yields a stress-induced birefringence whose axes are parallel and perpendicular to the plane of curvature, and thus do not rotate with twist. The beat length is given by $L_B = \lambda_0/\Delta n$, where λ_0 is the wavelength in vacuum and the refractive index difference $\Delta n = 0.133(r/R)^2$, where R is the bending radius and r the fibre radius [34,35]. Polarisation thus only rotates by $\sim 0.05N$ with respect to the birefringence axes in this case, so that the averaging out of birefringence is less effective. However, considering that the radius of curvature is not too small (say, 30 cm), a moderate twist rate of 1 turn/m can be sufficient to ensure nearly circular birefringence [24]. Taking for example $r = 62.5$ μm, $\lambda_0 = 1.55$ μm and $R = 30$ cm, one finds that the product $0.05NL_B \approx 13$ is still quite large. As we will show in this work that high twist induces substantial pulse distortion, we will consider a moderate twist rate of 1 turn/m for most calculations of this study. The electric field pulse envelope at the NOLM input is $E(z = 0, t) = A\,\mathrm{sec}\,h(1.763\,t/T_{FWHM})$, where T_{FWHM} is the full-width at half-maximum of the pulse power envelope.

The NPR-based NOLM scheme is presented in Fig. 1. It includes a 50/50 coupler, a piece of twisted (circularly birefringent) fibre

and a QWR located in the loop just after one of the coupler output ports. For a 1-km loop, the continuous-wave NOLM switching power $P_\pi = 6\pi/\gamma L = 2.51\,\mathrm{W}$. We consider circular (say, right) polarisation at the NOLM input. The CW beam is maintained circularly polarised during propagation, whereas the CCW beam is made linearly polarised through the QWR. Under these conditions, the continuous-wave transmission characteristic of the NOLM is a sinusoidal function of input power, whose dynamic range can be adjusted between 1 and ∞ when the QWR angle α is varied [26]. For two particular positions of the QWR, a wide plateau is obtained in the output power characteristic, which allowed in an experiment high-quality amplitude equalisation of subnanosecond pulses [29]. In the case of ultrashort pulses, when dispersion and group velocity mismatch play an important part, this behaviour remains qualitatively the same, as shown in Fig. 2(a and b), where transmission T and output pulse energy E_{out} are presented, as functions of input pulse energy E_{in}, for various values of the QWR angle, α. The transmission here is defined as the ratio between the pulse energies at the NOLM output and input, respectively, $T = E_{out}/E_{in}$. Fig. 2(b) shows that, for $\alpha = 0.89\pi/4$ and $\alpha = 1.09\pi/4$, a plateau appears in the E_{out} characteristic, where the first and second derivatives of the curve cancel out simultaneously. Both plateaus can be exploited to reduce large pulse energy fluctuations. The curve for $\alpha = 0.89\pi/4$ is much more attractive in practice, however, as the required input energy is substantially smaller than the other curve, so that this case will be analysed here. As it will be shown in this work, these curves, and in particular the plateau width, strongly depend on the input pulse characteristics.

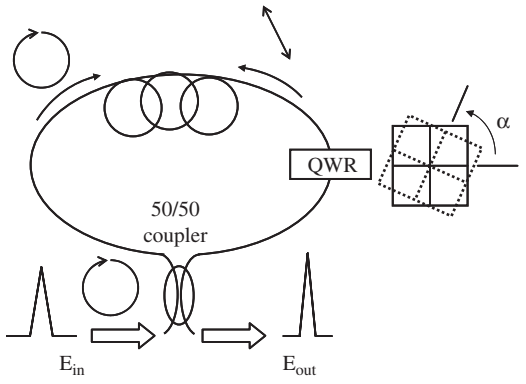

Fig. 1. Configuration under study. Conventionally, the QWR angle $\alpha = 0$ for infinite dynamic range.

Fig. 2(a and b) also shows that the curves depend on the value of twist. High twist still allows the existence of a plateau presenting essentially the same width, however the optimal adjustment angle depends on the value of twist. The dotted curves in Fig. 2(a and b) show that, for a twist of 6 turns/m, a flat plateau is no longer obtained for $\alpha = 0.89\pi/4$, however it is obtained for $\alpha = 0.85\pi/4$ (not shown on the figure). In practice however, high twist should be avoided, as the output pulse profile is distorted in this case (see Fig. 2(c)). This is due to the group velocity mismatch between circular left and right polarisation components. For a twist rate of 6 turns/m ($q = 12\pi$ rad/m), the refractive index mismatch $\Delta n = \lambda/\pi \times hq/2n \approx 10^{-6}$, where $\lambda = 1550$ nm is the wavelength, $h \approx 0.15$ and $n = 1.46$ is silica refractive index, which yields a delay $\Delta t = \Delta n/c \approx 3$ ps/km between the circular polarisation components ($c = 3 \times 10^8$ m/s is the velocity of light in vacuum). Fortunately, such a wide temporal separation between the polarisation components, comparable with the pulse width,

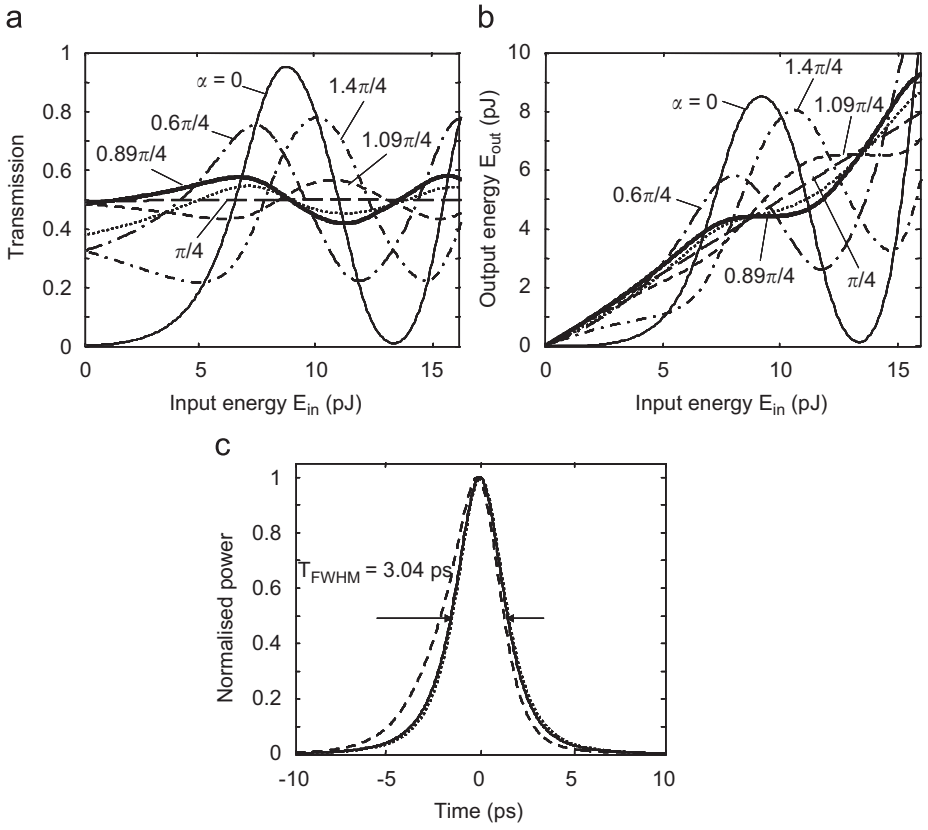

Fig. 2. Transmission (a) and output pulse energy (b) characteristics of the NPR-based NOLM, for various values of α (indicated as curve labels; $\alpha = 0$ for maximal dynamic range). An input pulse duration $T_{FWHM} = 2.65$ ps was chosen. Fibre twist = 6 turns/m (dotted) and 1 turn/m (all other curves); (c) output pulse profiles when α and E_{in} are adjusted to the plateau, for twist values of 0 (dotted), 1 (solid) and 6 turns/m (dashed).

does not appear at high power. In the case of the linearly polarised CCW beam, both circular polarisation components are equally excited. For the high pulse energies where the plateau appears in the E_{out} characteristic, both components remain bound together through the interplay between Kerr effect and anomalous dispersion [30], and both propagate at the average group velocity v_g. In the case of the CW beam, however, only one circular polarisation component (C^+) is excited, which propagates at the group velocity $v_g^+ = 1/\beta_1^+$. As both pulses recombine at the NOLM output, this mismatch translates into a substantial asymmetry of the switched pulse, and some increase of the output pulse duration. Fig. 2(c) shows that, for zero twist, the FWHM duration of the output pulse is 3.04 ps. For a twist of 6 turns/m, the duration is ~12% higher, whereas this increase is <1% for 1 turn/m (in this case, the pulse profile is little affected by twist).

Considering a twist rate of 1 turn/m, we analysed, for several values of the input pulse duration, the output energy characteristic (when α is adjusted in each case to get a plateau) and the characteristics of the switched pulses. The pulse duration T_{FWHM} ranged between 1 and 5.3 ps. Over this range, we observed that taking into account the Raman self-frequency shift in Eq. (1) did not alter significantly the results, so that its influence could be neglected. For $T_{FWHM} > 5.3$ ps, output pulse splitting started to occur when the input energy was raised up to the plateau region, due to the large value of the soliton order. Fig. 3(a) shows portions of the E_{out} curves for some values of T_{FWHM}. In each case, the QWR angle α is adjusted to get a flat plateau. The optimal value of α appeared to depend slightly on pulse duration, and ranged in all cases in an interval of ~6% around $\alpha = 0.9\pi/4$. This variability of the optimal adjustment with the input pulse characteristics illustrates an advantage of our scheme over the SPM-based scheme with large power imbalance [36], which also allows the existence of a wide plateau in the nonlinear characteristic, but does not allow adjusting the dynamic range (except if a coupler with adjustable coupling ratio is used).

Fig. 3(b), solid shows that, as expected, the plateau width is substantially wider than the simple maximum obtained when $\alpha = 0$, where only the first derivative of $E_{out} = 0$ (dashed curve, see also Fig. 2(b)). An important observation in Fig. 3(a and b) is that the width of the plateau strongly depends on the input pulse duration. The maximum width is obtained for $T_{FWHM} \approx 2.8$–3 ps, where amplitude fluctuations at the input as large as ~28% are reduced to 2% peak to peak in the switched signal. It turns out that the plateau widens substantially when the pulses injected at both ends of the loop (each corresponding to half the input pulse energy) are close to solitons at the energy of the plateau. Solid curves in Fig. 3(c) show the soliton order N for input CW and CCW pulses as a function of input pulse duration, when the input pulse energy is adjusted in each case to the plateau centre. Note that, even if the counter-propagating pulses have the same duration and peak power when they enter the loop (due to the 50/50 coupler), they have different values of N, because of their different polarisation states. Indeed, the nonlinear coefficient for the linearly polarised CCW beam is 3/2 times higher than that of the circularly polarised CW beam (this can be easily verified if one considers that a linearly polarised field E is composed of two

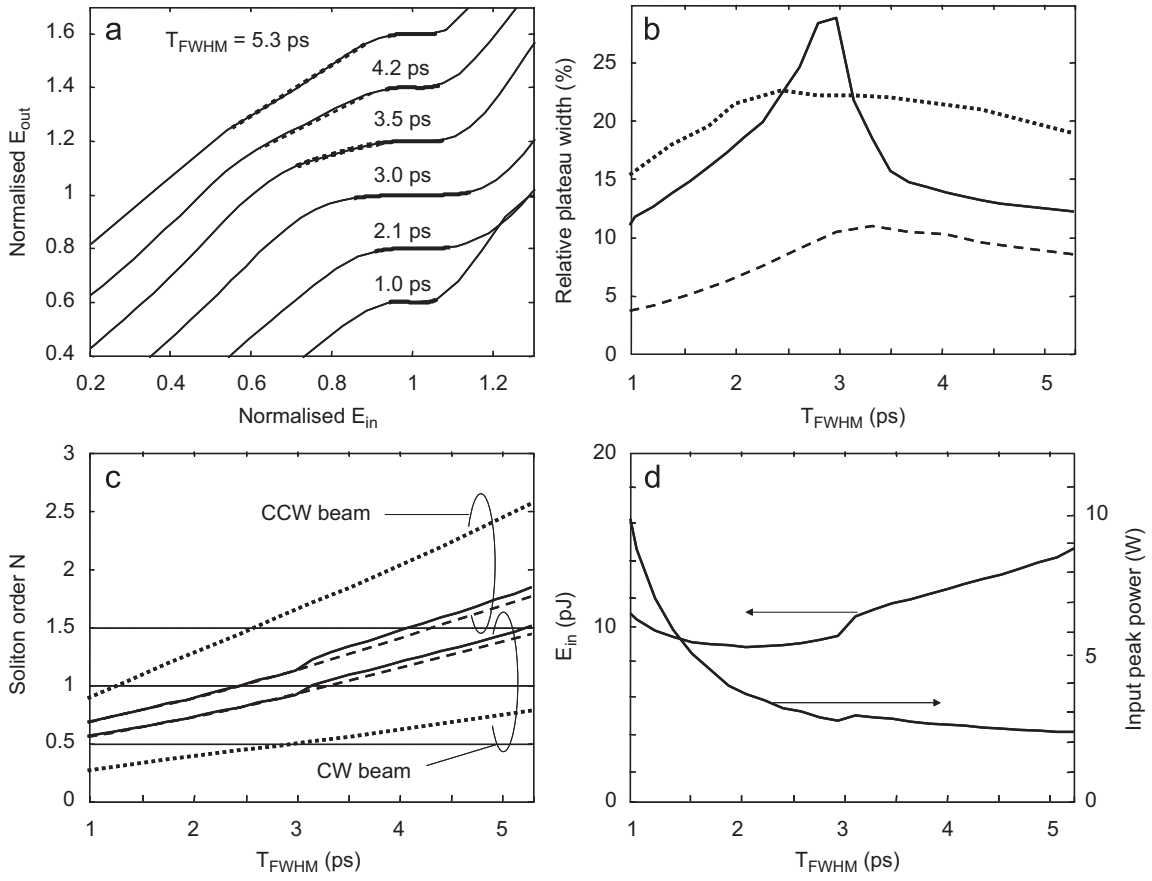

Fig. 3. (a) Normalised E_{out} characteristics when α is adjusted to form a plateau, for several values of input pulse duration T_{FWHM} (shown as curve labels); curves were shifted vertically for better readability; (b) relative width of the plateau (solid) and of the maximum of E_{out} when $\alpha = 0$ (dashed) for the NPR-based NOLM, and width of the plateau of the large-power-imbalanced NOLM (dotted); this width is defined for each T_{FWHM} as the E_{in} interval over which E_{out} varies within $\pm 1\%$, and is normalised to the value of E_{in} at the plateau centre; (c) soliton order N of injected CW and CCW beams, in function of T_{FWHM}, for the NPR-based NOLM when α is adjusted to form a plateau (solid), when $\alpha = 0$ (dashed), and for the large-power-imbalanced NOLM (dotted); (d) E_{in} and input peak power at the plateau centre in function of T_{FWHM}.

circular components C^+ and C^- of equal amplitudes, yielding $|E|^2 = |C^+|^2+|C^-|^2 = 2|C^+|^2 = 2|C^-|^2$, so that the nonlinear coefficients of the last terms in Eq. (1) can be written as $\gamma|E|^2$). As a result, the soliton order is $\sqrt{3/2}$ times higher for linear polarisation than for circular polarisation, assuming the same pulse profile and peak power. It appears from Fig. 3(b) and (c) that the plateau width is maximal for pulse durations corresponding to soliton orders close to 1 ($N_{CW}<1<N_{CCW}$ for $2.5\,ps<T_{FWHM}<3.2\,ps$). Within this range, considering that the loop length includes several soliton periods ($Z_0=\pi T_{FWHM}^2/|\beta_2|/6.21\approx180\,m$ for $T_{FWHM}=3\,ps$ and parameters of this study), both pulses quickly evolve towards solitons with minor adjustments of their parameters. In this case, both pulses propagate as nearly fundamental solitons practically over the whole fibre length. So the substantial widening of the plateau that occurs over this range of pulse duration appears to be a manifestation of the outstanding stability of solitons to small variations of pulse parameters [30]. For larger pulse durations, however, the main part of the former plateau acquires a positive slope, whereas only its upper end is maintained horizontal (see Fig. 3(a) for $T_{FWHM}\geqslant3.5\,ps$, thick dashed). This occurs as the N parameter at the plateau becomes >1 for both CW and CCW beams (see Fig. 3(c)). In particular, the CCW pulse undergoes important readjustments to match the fundamental soliton (as far as $N_{CCW}<1.5$), a process which may be uncompleted at the fibre end (Z_0 being larger for larger pulse duration). This evolution corresponds to a sudden increase of the plateau centre as the pulse width grows beyond $T_{FWHM}=3\,ps$, this jump is visible in Fig. 3(d). Symmetrically, the plateau is shortened for small values of pulse duration, in which case N_{CW} and $N_{CCW}<1$, and important readjustments are at play in particular for the CW pulse (although Z_0 is smaller in this case, simulations show that the profile converges to a soliton only after $\sim$500 m for $T_{FWHM}=1\,ps$, due to the importance of the readjustments). So it appears that the plateau widens substantially only when both pulses behave as fundamental solitons over an extended section of the fibre span.

As a comparison, we also determined numerically the plateau width in the case of a large-power-imbalanced NOLM [36]. It consisted of a $\sim$0.91/0.09 coupler and a section of the same fibre as the NPR-based NOLM (although untwisted). Polarisation was assumed to be linear (i.e., polarisation effects were not considered). The loop length, $L\approx200\,m$, was chosen so that the switching power would be the same as the NPR-based NOLM. In order to maintain a flat plateau in the nonlinear characteristic for all values of input pulse duration, the coupling ratio of the coupler was slightly adjusted around 0.91/0.09 in each case. These results are included in Fig. 3(b), dotted curve. It appears that the maximal plateau width is lower in this case: $\sim$22% for $T_{FWHM}\approx2.5\,ps$, a value comparable with the one found experimentally in [36, Fig. 1]. This can be understood by considering that, due to the large power imbalance of this scheme, the soliton orders of the counter-propagating pulses are always very different (Fig. 3(c), dotted curves). Besides, considering that the pulse will evolve towards a fundamental soliton only if $0.5<N<1.5$, it comes from observing Fig. 3(c) that the CW and CCW pulses will never evolve simultaneously towards first-order solitons. It has to be noted however that, unlike the proposed scheme, the plateau width for the large-power-imbalanced NOLM only slightly varies with input pulse duration, and remains at a value close to the maximum ($>20\%$) over a wide range of T_{FWHM}.

Finally, Fig. 3(d) shows that the input pulse energy at the plateau is quite constant over the range of pulse duration $1.5\,ps<T_{FWHM}<3\,ps$, with a slight parabolic dependence related to the dispersive wave that builds up when the input pulse parameters deviate from the ideal soliton parameters [30]. Correspondingly to this nearly constant E_{in} characteristic, input peak power is roughly inversely proportional to pulse duration. In practice, input peak powers of a few watts are compatible with the power levels that can be produced using currently available optical communication technology, even in the case of rather high signal duty ratio. In particular, the signal can be obtained from ultrashort pulse trains produced by semiconductor laser diodes or mode-locked fibre lasers. If the signal power is boosted by an erbium-doped fibre amplifier, average powers as high as several hundreds of milliwatts can be obtained [4,12]. Assuming for example an ultrashort-pulsed signal at 40 Gb/s presenting a duty ratio of 0.1, peak powers of a few watts are readily obtained.

Fig. 4 shows some characteristics of the switched pulses when their input energy is matched to the plateau, as functions of pulse duration. Fig. 4(a) presents the soliton order N of the output pulses. As those appeared to be nearly circularly polarised, N was calculated using the nonlinear coefficient for circular polarisation, $2/3\gamma$ (thin solid). The N curve obtained using γ as the nonlinear coefficient is also presented (thick solid), as the circular right polarisation of the pulses can be easily made linear using a QWR at the NOLM output. The values of N in the latter case are very close to 1, like in the case of the large-power-imbalance NOLM (dotted curve). This feature is interesting, in particular if we compare with the case of a conventional NOLM using a slightly power-imbalanced coupler: if the counter-propagating pulses evolve towards fundamental solitons ($N\approx1$) in the loop, at switching, where transmission is close to 1 and the fields add up in phase, the output peak power is about twice the peak power of the individual pulses, leading to a soliton parameter close to $\sqrt{2}$, thus substantially higher than 1 [37, Fig. 2]. Note that this also happens for the NPR-based NOLM when $\alpha=0$, as in this case the maximal transmission is also close to 1 (Fig. 4(a), dashed). In contrast, when α is adjusted to get a plateau, the output soliton parameter close to 1 can be related to the fact that, at the plateau, the NOLM transmission is about 0.5 (see Fig. 2(a)).

Fig. 4(b) (solid) shows the output pulse "pedestal", calculated as the relative difference in modules between the output pulse energy and the energy of the squared hyperbolic secant pulse having the same T_{FWHM} and peak power as the actual pulse. This pedestal is related to the dispersive waves that form when the pulses injected in the loop depart from fundamental solitons. The nearly parabolic shape of the curve is coherent with the results of soliton perturbation theory [30]. The smaller pedestal values are observed in the range where the soliton orders are close to 1, with a minimal value of $\sim$5% for $T_{FWHM}=3\,ps$. The formation of dispersive waves cannot be avoided, however, for any value of input pulse duration, as the soliton parameters of the injected beams cannot be $=1$ simultaneously (Fig. 3(c)). These dispersive waves are switched to the NOLM output, together with the soliton part, as low-power transmission is high when a plateau is formed in the E_{out} characteristic, and no pedestal suppression takes place (Fig. 2(a)). In spite of this, the minimal values of a few % obtained when the plateau width is maximal still support the comparison with the performances of the NOLM when $\alpha=0$ (dashed curve in Fig. 4(b)), or with conventional NOLMs close to the switching power [37, Fig. 1], although in these cases low-power transmission is small. In the case of the large-power-imbalance NOLM (dotted curve in Fig. 4(b)), the pedestal values when the plateau width is maximal ($T_{FWHM}\approx2.5\,ps$) are also of a few % only, in spite of the initial values of N that strongly depart from 1 in this case (Fig. 3(c)). This has to be related to the short loop length of this NOLM, which does not allow the dispersive wave to develop completely.

Fig. 4(c) presents the dependence of output versus input pulse durations. For short input pulse duration, the soliton order at the fibre input is <1 for both pulses (Fig. 3(c)), hence their duration increases during propagation so as to increase the soliton order [30].

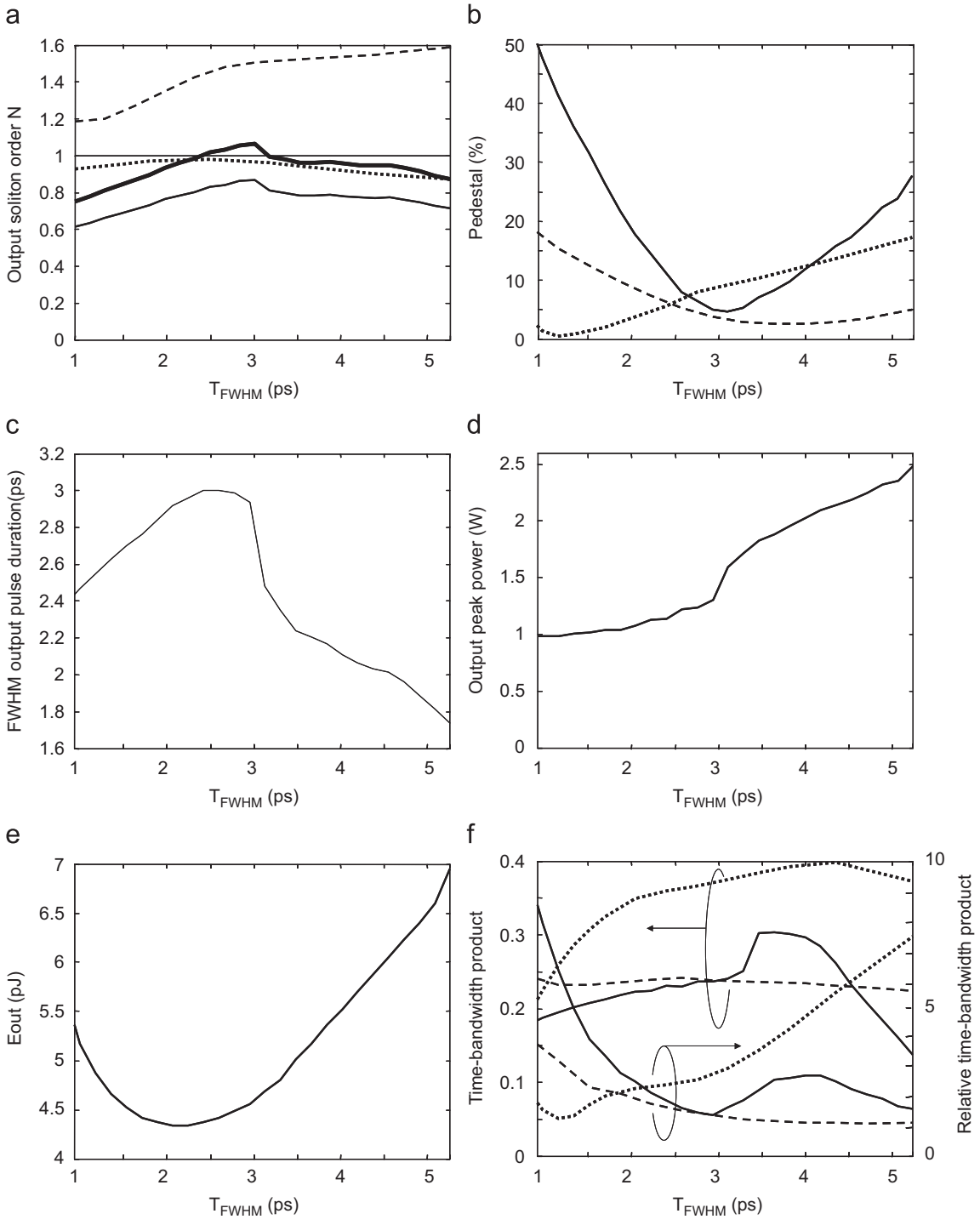

Fig. 4. (a) Output soliton number assuming circular (thin solid) and linear (thick solid) polarisations; (b) "pedestal", (c) FWHM duration, (d) peak power and (e) energy of the output pulses; (f) time-bandwidth product of the output pulses and ratio between that product and the time-bandwidth product of the corresponding transform-limited pulses. Dashed and dotted curves in (a), (b) and (f) are related to the NPR-based NOLM with $\alpha = 0$ and to the large-power-imbalance NOLM, respectively.

As a consequence, the pulse duration at the NOLM output is larger than at the input. For 2.5 ps $< T_{FWHM} <$ 3.2 ps, the soliton order is <1 for the CW pulse and >1 for the CCW pulse, so that the pulse durations slightly increase and decrease during propagation, respectively, and the switched pulse duration is nearly identical to the input duration. For wider input pulses, the soliton order is >1 for both pulses, which leads to pulse shortening and yields an output pulse shorter than the input pulse.

Fig. 4(d) and (e) show the dependences of output peak power and pulse energy, respectively, on input pulse duration. These parameters, like the output pulse duration (Fig. 4(c)), are nearly constant near the maximal plateau width ($T_{FWHM} = 2$–3 ps). These results confirm that, over a relatively wide range of input pulse duration, when the input energy is adjusted at the plateau, solitons tend to form during the propagation in the loop in each direction and, when they recombine at the coupler, their duration and peak power are roughly independent of their initial values. This can be understood by considering that the nonlinear phase shift of solitons is proportional to their peak power, and that the plateau appears for a particular value of the nonlinear phase shift

difference between counter-propagating beams ($\sim 1.2\pi$ as determined in [29]). Considering that the soliton period is substantially shorter than the loop length, peak powers of solitons at the plateau are then imposed by the condition that their nonlinear phase shift difference be $\sim 1.2\pi$. Over the range $2.5\,\text{ps} < T_{\text{FWHM}} < 3$ ps, Figs. 3(d) and 4(d) show that the output peak power is nearly half the input peak power, which confirms that the pulses suffered little reshaping during propagation [the NOLM transmission at the plateau is ~0.5 in all cases, see Fig. 2(a and b)]. Shorter input pulses widen during propagation, so that their peak power diminishes, and the opposite happens for larger input pulses, so that higher input peak power is associated with lower output peak power, and conversely, so as to maintain in all cases the overall phase shift difference $\sim 1.2\pi$. Finally, the slight parabolic dependence of output pulse energy on the pulse duration (Fig. 4(e)) has to be related to the same dependence already observed in E_{in} (Fig. 3(d)).

Fig. 4(f) (solid) presents the dependence of the time-bandwidth product of output pulses. Also shown in the figure is the ratio between the time-bandwidth product and the time-bandwidth product of the transform-limited pulses having the same temporal profile as the actual output pulses. The figure shows that, over the range of $2.5\,\text{ps} < T_{\text{FWHM}} < 3$ ps, output pulses are nearly transform-limited, but the time-bandwidth product is smaller than the expected value of ~0.31 for transform-limited squared hyperbolic secant pulses. This also happens for conventional NOLMs near switching [37], and can be attributed to the effect of the dispersive wave, which tends to narrow the spectrum linewidth. For $T_{\text{FWHM}} = 3$ ps, very similar values are obtained for the NPR-based NOLM with $\alpha = 0$ (dashed lines). In comparison, the pulses from the large-power-imbalance NOLM substantially depart from the transform limit when the plateau width is maximal ($T_{\text{FWHM}} = 2.5$ ps, dotted curves). Note finally the steep transitions that are visible in Fig. 4(a, c, d and f) near $T_{\text{FWHM}} = 3$ ps, related to the jump in the plateau energy of the NPR-based NOLM that occurs around that pulse duration (Fig. 3(d)).

From the analysis of Fig. 4, it appears that the operation of the NPR-based NOLM used as pulse energy equaliser is optimal when the soliton numbers of the pulses injected into the loop are close to 1. Note that this means that the soliton number of the input pulses should be close to 2, which implies a previous amplification of the input pulses if those are close to fundamental solitons. Equalisation of energy fluctuations as high as ~25–30% is possible over some range of input pulse duration ($2.5\,\text{ps} < T_{\text{FWHM}} < 3$ ps for the parameters of this study), and yields nearly chirp-free pulses close to fundamental solitons, with a pedestal not higher than a few %. Outside this range, however, important pulse reshaping takes place, and the plateau is very narrow, allowing the equalisation of energy fluctuations not higher than 10–15%, at the price of a high chirp and a large pedestal affecting the output pulses. In particular, for larger pulses, a different NOLM should be used, for example implementing a longer loop of the same fibre, or the same length of a fibre having higher dispersion, in order to maintain the soliton parameter close to 1 for the counter-propagating pulses. When the input pulses are Gaussian instead of solitons, the device performances are roughly the same, except that the pulse duration for maximal plateau extension is slightly modified (~2.6 ps), as well as the optimal adjustments of the QWR angle. In particular, around this optimal pulse duration, the plateau extension is not reduced as compared to the sech^2 case, and the output pedestal remains limited to a few %, in spite of the additional readjustments that take place when the pulses evolve towards ideal solitons.

When the duty ratio of the signal (and thus its mean power) is large, as it occurs at very high bit rates, the operation of a NOLM can be severely affected by the cross-phase modulation (XPM) between counter-propagating beams [4,23,38–40]. In conventional self-switched devices, the counter-propagating interaction is responsible for the appearance of a phase bias in the transmission characteristic, which is proportional to the signal mean power. As a result, low-power transmission is no longer minimal, and the switching power is increased [40]. In the case of the NPR-based NOLM, one should consider that the nonlinear phase shift coefficients resulting from XPM between parallel and orthogonal polarisation components are different [30]. In the particular case of circular birefringence, however, these coefficients become equal, and considering that the counter-propagating beams have equal powers, it comes that the XPM phase shifts undergone by the CW and CCW beams are equal. As a consequence, these phase shifts cancel out at the NOLM output, and the NOLM operation is not altered with respect to the case of low-duty-ratio signals. If now fibre birefringence is not perfectly circular, the phase shifts induced by XPM no longer cancel out, and the transmission curve is affected. For the QWR angle adjustment corresponding to a plateau under low-duty-ratio signals, a plateau is no longer observed in the case of a high-duty-ratio signal. A plateau can still be found however for a different adjustment of the QWR angle. The plateau power is slightly increased, however, as a result of the phase bias. The maximal plateau width is similar to the case of low-duty-ratio signals, although this maximum occurs for slightly smaller pulse durations, as a consequence of the increase in the plateau power.

3. Conclusion

We studied numerically the NPR-based NOLM for reduction of large amplitude fluctuations of an ultrashort-pulsed optical signal. For circular input polarisation, when the orientation of the QWR inserted in the loop is properly adjusted, a flat plateau appears in the output power characteristic. We showed that, thanks to the interplay between anomalous dispersion and Kerr nonlinearity, the impairments caused by the group velocity mismatch between circular polarisation components of the ultrashort pulses are minor for moderate values of twist. Our analysis also showed that, when the parameters of the input pulses injected in the loop are close to those of a fundamental soliton in both directions, a substantial enhancement of the plateau width occurs. In this case, amplitude fluctuations as large as 28% can be reduced to less than 2% using this scheme. As a comparison, this maximum reduces to ~22% if a large-power-imbalance NOLM with the same switching energy is used. The output pulses are close to transform-limited, first-order solitons, although their time-bandwidth product is slightly smaller than the one of ideal solitons, due to the existence of a dispersive wave which amounts to ~5% of the total pulse energy. When the input pulses are not close to solitons, however, the plateau width is substantially smaller, the output pulses are strongly chirped and are accompanied by a strong pedestal. This emphasises that the NOLM parameters should be adapted to the particular pulse parameters for proper regeneration operation. The device has the potential to realise tasks such as enhancement of very low signal-to-noise ratio in ultrafast transmission systems.

Acknowledgement

O. Pottiez was supported by CONACyT Grant 53990.

References

[1] Doran NJ, Wood D. Nonlinear optical loop mirror. Opt Lett 1988;13:56–8.
[2] Sotobayashi H, Sawaguchi C, Koyamada Y, Chujo W. Ultrafast walk-off-free nonlinear optical loop mirror by a simplified configuration for 320-Gbit/s time-division multiplexing signal demultiplexing. Opt Lett 2002;27:1555–7.

[3] Lee JH, Tanemura T, Takushima Y, Kikuchi K. All-optical 80-Gb/s add-drop multiplexer using fiber-based nonlinear optical loop mirror. IEEE Photon Technol Lett 2005;17:840–2.
[4] Sakamoto T, Kikuchi K. 160-Gb/s operation of nonlinear optical loop-mirror with an optical bias controller. IEEE Photon Technol Lett 2005;17:1058–60.
[5] Pelusi MD, Matsui Y, Suzuki A. Pedestal suppression from compressed femtosecond pulses using a nonlinear fiber loop mirror. IEEE J Quantum Electron 1999;35:867–74.
[6] Attygalle M, Nirmalathas A, Liu HF. Novel technique for reduction of amplitude modulation of pulse trains generated by subharmonic synchronous mode-locked laser. IEEE Photon Technol Lett 2002;14:543–5.
[7] Bogoni A, Ghelfi P, Scaffardi M, Potí L. All-optical regeneration and demultiplexing for 160-Gb/s transmission systems using a NOLM-based three-stage scheme. IEEE J Sel Topics Quantum Electron 2004;10:192–6.
[8] Boscolo S, Turitsyn SK. All-optical nonlinear pulse processing based on normal dispersion fiber-enhanced nonlinear optical loop mirror. IEEE Photon Technol Lett 2004;16:1912–4.
[9] Cvecek K, Onishchukov G, Sponsel K, Striegler AG, Schmauss B, Leuchs G. Experimental investigation of a modified NOLM for phase-encoded signal regeneration. IEEE Photon Technol Lett 2006;18:1801–3.
[10] Bogoni A, Poti L, Proietti R, Meloni G, Ponzini F, Ghelfi P. Regenerative and reconfigurable all-optical logic gates for ultra-fast applications. Electron Lett 2005;41:435–6.
[11] Oda S, Maruta A. All-optical digital-to-analog conversion using nonlinear optical loop mirrors. IEEE Photon Technol Lett 2006;18:703–5.
[12] Adams R, Rochette M, Ng TT, Eggleton BJ. All-optical in-band OSNR monitoring at 40 Gb/s using a nonlinear optical loop mirror. IEEE Photon Technol Lett 2006;18:469–71.
[13] Islam MN, Sunderman ER, Stolen RH, Pleibel W, Simpson JR. Soliton switching in fiber nonlinear loop mirror. Opt Lett 1989;14:811–3.
[14] Chusseau L, Delevaque E. 250-fs optical pulse generation by simultaneous soliton compression and shaping in a nonlinear optical loop mirror including a weak attenuation. Opt Lett 1994;19:734–6.
[15] Wong WS, Namiki S, Margalit M, Haus HA, Ippen EP. Self-switching of optical pulses in dispersion-imbalanced nonlinear loop mirrors. Opt Lett 1997;22:1150–2.
[16] Khrushtchev IY, White IH, Penty RV. High-quality laser diode pulse compression in dispersion-imbalanced loop mirror. Electron Lett 1998;34:1009–10.
[17] Moores JD, Bergman K, Haus HA, Ippen EP. Optical switching using fiber ring reflectors. J Opt Soc Am B 1991;8:594–601.
[18] Smith NJ, Doran NJ. Picosecond soliton transmission using concatenated nonlinear optical loop-mirror intensity filters. J Opt Soc Am B 1995;12:1117–25.
[19] Finlayson N, Nayar BK, Doran NJ. Switch inversion and polarization sensitivity of the nonlinear-optical loop mirror. Opt Lett 1992;17:112–4.
[20] Baskev Clausen C, Povlsen JH, Rottwitt K. Polarization sensitivity of the nonlinear amplifying loop mirror. Opt Lett 1996;21:1535–7.
[21] Kuzin EA, Korneev N, Haus JW, Ibarra-Escamilla B. Theory of nonlinear loop mirrors with twisted low-birefringence fiber. J Opt Soc Am B 2001;18:919–25.
[22] Lin Q, Agrawal GP. Impact of fiber birefringence on optical switching with nonlinear optical loop mirrors. IEEE J Sel Topics Quantum Electron 2004;10:1107–14.
[23] Bogoni A, Scaffardi M, Ghelfi P, Potí L. Nonlinear optical loop mirrors: investigation solution and experimental validation for undesirable counter-propagating effects in all-optical signal processing. IEEE J Sel Topics Quantum Electron 2004;10:1115–23.
[24] Tanemura T, Kikuchi K. Circular-birefringence fiber for nonlinear optical signal processing. J Lightwave Technol 2006;24:4108–19.
[25] Feldman SF, Weinberger DA, Winful HG. Polarization instability in a twisted birefringent optical fiber. J Opt Soc Am B 1993;10:1191–201.
[26] Pottiez O, Kuzin EA, Ibarra-Escamilla B, Mendez-Martinez F. Theoretical investigation of the NOLM with highly twisted fibre and a $\lambda/4$ birefringence bias. Opt Commun 2005;254:152–67.
[27] Ibarra-Escamilla B, Kuzin EA, Zaca-Morán P, Grajales-Coutiño R, Mendez-Martínez F, Pottiez O, et al. Experimental investigation of the nonlinear optical loop mirror with twisted fiber and birefringence bias. Opt Express 2005;13:10760–7.
[28] Pottiez O, Kuzin EA, Ibarra-Escamilla B, Camas-Anzueto JT, Gutiérrez-Zainos F. Easily tunable nonlinear optical loop mirror based on polarization asymmetry. Opt Express 2007;12:3878–87.
[29] Pottiez O, Kuzin EA, Ibarra-Escamilla B, Gutiérrez-Zainos F, Ruiz-Corona U, Camas-Anzueto JT. High-order amplitude regularization of an optical pulse train using a power-symmetric NOLM with adjustable contrast. IEEE Photon Technol Lett 2005;17:154–6.
[30] Agrawal GP. Nonlinear fiber optics. 3rd ed. San Diego: Academic Press; 2001.
[31] Galtarossa A, Palmery L, Schiano M, Tambosso T. Measurements of beat length and perturbation length in long single-mode fibers. Opt Lett 2000;25:384–6.
[32] Kuzin EA, Estudillo-Ayala JM, Ibarra-Escamilla B, Haus JW. Measurements of beat length in short low-birefringence fibers. Opt Lett 2001;26:1134–6.
[33] Ulrich R, Simon A. Polarization optics of twisted single-mode fibers. Appl Opt 1979;18:2241–51.
[34] Lefevre HC. Single-mode fibre fractional wave devices and polarization controllers. Electron Lett 1980;16:778–80.
[35] Ulrich R, Rashleigh C, Eickhoff W. Bending-induced birefringence in single-mode fibers. Opt Lett 1980;5:273–5.
[36] Meissner M, Rösch M, Schmauss B, Leuchs G. 12 dB of noise reduction by a NOLM-based 2-R regenerator. IEEE Photon Technol Lett 2003;15:1297–9.
[37] Cao W, Wai PKA. Comparison of fiber-based Sagnac interferometers for self-switching of optical pulses. Opt Commun 2005;245:177–86.
[38] Jinno M, Matsumoto T. Nonlinear Sagnac interferometer switch and its applications. IEEE J Quantum Electron 1992;28:875–82.
[39] Arahira S, Murai H, Ogawa Y. Modified NOLM for stable and improved 2R operation at ultra-high bit rates. IEICE Trans Commun 2006;E89-B:3296–305.
[40] Pitois S. Influence of cross-phase modulation in SPM-based nonlinear optical loop mirror. Opt Commun 2005;253:332–7.